Seismological support for the metastable superplume model, sharp features, and phase changes within the lower mantle

Daoyuan Sun, Eh Tan*, Don Helmberger†, and Michael Gurnis

Seismological Laboratory, 252-21, California Institute of Technology, Pasadena, CA 91125

Edited by Russell J. Hemley, Carnegie Institute of Washington, Washington, DC, and approved March 7, 2007 (received for review September 15, 2006)

Recently, a metastable thermal-chemical convection model was proposed to explain the African Superplume. Its bulk tabular shape remains relatively stable while its interior undergoes significant stirring with low-velocity conduits along its edges and down-welling near the middle. Here, we perform a mapping of chemistry and temperature into P and S velocity variations and replace a seismically derived structure with this hybrid model. Synthetic seismogram sections generated for this 2D model are then compared directly with corresponding seismic observations of P (P, P_CP, and PKP) and S (S, S_CS, and SKS) phases. These results explain the anticorrelation between the bulk velocity and shear velocity and the sharpness and level of SKS travel time delays. In addition, we present evidence for the existence of a D'' triplication (a putative phase change) beneath the down-welling structure.

core-mantle boundary | D″

The large-scale structure of the lower mantle has been well resolved by global tomography, with a belt of high seismic velocity along the circum-Pacific and two large low velocity provinces (LLVPs) beneath South Africa and the mid-Pacific. The fastest regions appear to contain a sharp positive velocity jump associated with a phase-change from perovskite (PV) to postperovskite (PPV) (1), whereas the slowest regions contain a $\delta V_S/\delta V_P$ ratio >2.5 and an anticorrelated bulk sound velocity V_ϕ and shear velocity V_S (2, 3). Although both LLVPs show these properties, their interior structures appear to differ, with the Pacific anomaly showing more complexity compared with the apparently monolithic African anomaly (4, 5). Tomographic studies of the African structure reveal a large-scale feature that extends throughout the lower mantle. Predicted SKS delay patterns up to 3 s for some of these tomographic models fit the observations at the South African seismic array well except for magnitude and sharpness (Fig. 1), where the data require >6-s offsets (5, 6). Note that the SKS ray paths cross the core-mantle boundary (CMB) interface at relatively steep angles and their abrupt change in delays require nearly vertical walls to separate the normal Preliminary Reference Earth Model (PREM) from the anomalous structure denoted by the heavy green lines in Fig. 1*b* (reviewed in ref. 5). Such a structure with its sharp sides is suggestive of thermo-chemical convection containing a density increase (7).

Metastable Superplume

The fate of a dense chemical basal layer in a convecting mantle has a well developed history. The results from Christensen (8) and McNamara and Zhong (9), involving dense piles, look similar to the LLVPs in tomographic locations and appear compatible with the history of subduction. Stabilized by an intrinsically larger density ($\Delta\rho_{ch}$), the pile will remain at the CMB until exceeded by a thermal density with opposite sign ($\Delta\rho_{th}$). However, if there is a difference in compressibility between the material within the plume compared with ambient mantle, then metastable conditions are possible. Tan and Gurnis (10) have generated a sequence of models with differences in zero pressure density ($\Delta\rho_o$), adiabatic bulk modulus (K_s), and initial layer thickness. They show that if $\Delta\rho_o$ is 2–3% and K_s is 4–8% larger than the ambient mantle, which are expected for material from subducted slabs (pyroxenite)[‡], then metastable superplumes can form. The result that best matches the seismic data for the African Superplume, High Bulk Modulus Structure (HBMS), is used in our subsequent analysis (Fig. 2).

At the base of the mantle, the anomalous material heats, becomes more buoyant than the background, and moves upward. However, during ascent, its buoyancy gradually decreases, because of an increasing adiabatic density difference, and rises to a level where it is neutrally buoyant, height of neutral buoyancy (HNB). Above the HNB, the anomalous material becomes denser than the background and sinks. The structure stands high above the CMB (Fig. 2) and remains metastable depending on the equation of state and depth dependence of the coefficient of thermal expansion (10).

The existing seismic model of the African Low Velocity Structure (ALVS; Fig. 1) is similar in shape to the dynamic models but lacks smaller scale complexity and low seismic velocities near the edges. Such features are in some of the seismic models presented by Wen (12). The earlier idealized seismic structure (Fig. 1*b*) has a uniform 3% V_S reduction with walls and a flat roof, so that the general character of the anomaly might be imaged more clearly with waveform data available, transforming the blurry tomographic model into this distinct structure (13). We convert the temperature, composition, and density anomalies in the HBMS model to seismic velocity anomalies in favoring the bulk properties of the seismic African Superplume model [supporting information (SI) *Text*]. The thermo-elastic parameters of the chemical anomalous material are chosen to be similar to those of $MgSiO_3$ PV (14).

Predicting Seismograms

Here, synthetic seismograms generated from dynamically derived V_S and V_P models are tested against observed seismic phases and travel times. To test the HBMS model, we replace the

Author contributions: D.S. performed research; E.T., D.H., and M.G. contributed new reagents/analytic tools; and D.H. wrote the paper.

The authors declare no conflict of interest.

This article is a PNAS Direct Submission.

Abbreviations: LLVP, large low velocity province; PV, perovskite; PPV, postperovskite; CMB, core-mantle boundary; PREM, Preliminary Reference Earth Model; HBMS, High Bulk Modulus Structure; ALVS, African Low Velocity Structure; P_d, P-wave diffraction; S_d, S-wave diffraction.

*Present address: Computational Infrastructure for Geodynamics, 220-12, California Institute of Technology, Pasadena, CA 91125.

†To whom correspondence should be addressed. E-mail: helm@gps.caltech.edu.

‡Lee, K.K., Asimow, P.D., Tschauner, O. (2005) *EOS Trans AGU* 86:V42A-02 (abstr.).

This article contains supporting information online at www.pnas.org/cgi/content/full/0608160104/DC1.

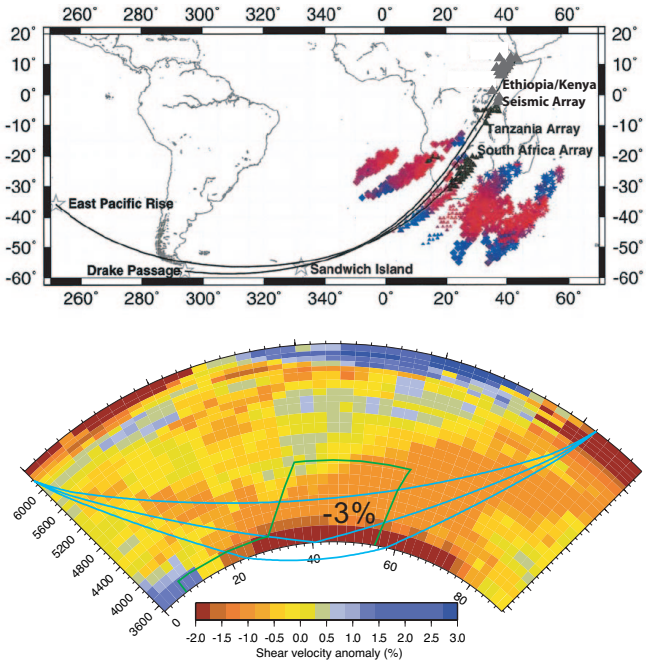

Fig. 1. A map of events and stations (triangles) used in the construction of a 2D model along a corridor through the African Superplume. We use data from two arrays, South African and the new Ethiopia/Kenya array (19) of events arriving along a great circle in this study. SKS and SKKS exist points at the CMB are given in colored triangles, with blue indicating no delay and red >5 s. To produce the sharp jumps requires a monolithic structure denoted in heavy green lines as the ALVS, where the S velocity inside the box is reduced by 3% relative to PREM (18). We have included some example ray paths S, SKS, and S_CS. The background tomographic model is the most recently updated Grand model (27).

box-like structure (Fig. 1*b*) with the HBMS structure (Fig. 3*a*), while assuming the same geometry and then generate 2D synthetics (15). Then, we compare the predicted synthetic seismograms with the data. Specifically, (*i*) does HBMS display the sudden jump in SKS at the edges and remain relatively flat over extended distances while generating complex SKS waveform when sampling the edges? (*ii*) Does HBMS satisfy the travel time data S-wave diffraction (S_d) and P-wave diffraction (P_d), where S_d is delayed much more than P_d? (*iii*) Does it predict the much larger delayed S_CS-S than P_CP-P? We find that HBMS predicts the bulk characteristics about as well as the idealized seismic model (Fig. 1*b*) but also predicts small-scale features near the edges and middle, which can be seen in the observed waveform data.

Although the early waveform studies of the African Superplume revealed sharp features based on differential phase relationships (SKS-S and S-S_CS) (6, 13, 16), the dense regional array data provided the most definitive evidence (17). Thus, we will concentrate on array data and 2D synthetics generated from events along the great circle paths displayed in Fig. 1*a*. Synthetic waveforms for the HBMS model are processed by using the same procedure as used in deriving Fig. 1*b*, with results displayed in Fig. 3. We also included reversed paths or flipping the HBMS model because the detailed velocity field is not unique, i.e., changes with time, etc. The HBMS results fit as well as ALVS although a few seconds of scatter remain. The synthetics are displayed in SI Fig. 7 where complexities develop near the boundary as can be observed (7), but these features remain difficult to quantify.

Long-period P_d that passes through the African anomaly is less delayed than S_d from conventional tomography. This feature is

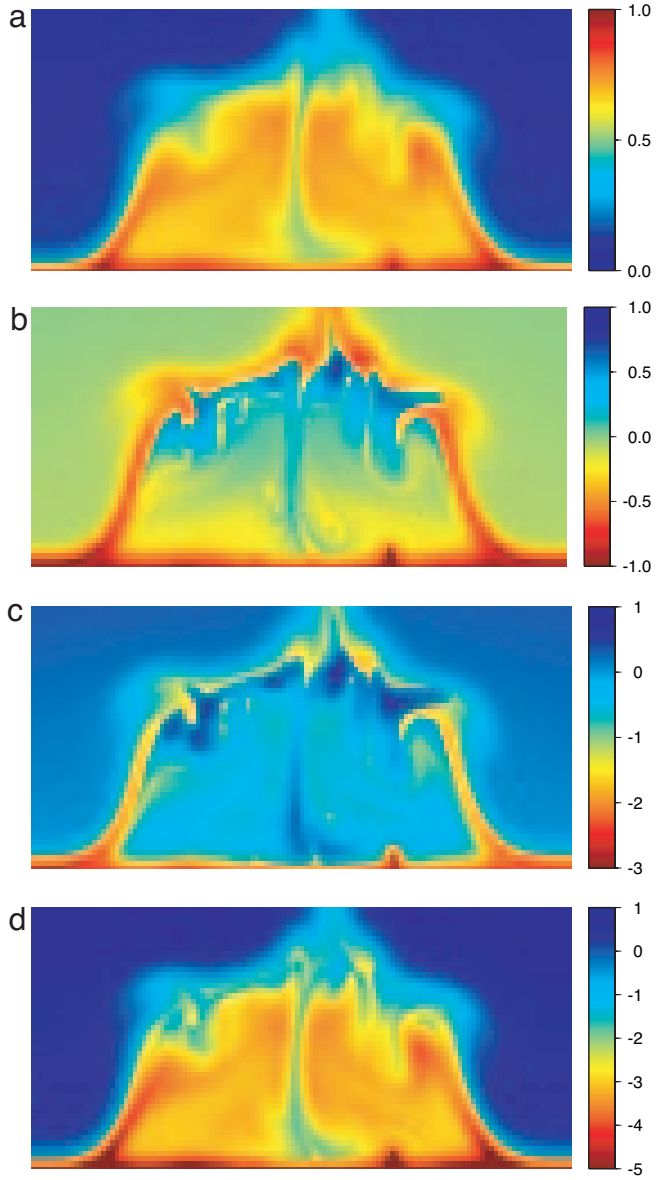

Fig. 2. Display of a 2D section through a metastable thermo-chemical structure along with predicted V_P and V_S velocities (14). Only the bottom 1,200 km of the model is shown. Within the anomaly, the material has a larger bulk modulus (6% larger than ambient) and higher zero pressure density (2.25%). The layer forms a single dynamic structure with the average density near neutral. Note the plumes along the edges and the down-welling near the middle. (*a*) Nondimensional temperature. (*b*) Density anomaly, $\delta\rho$ (%). (*c*) V_P anomaly, δV_P (%). (*d*) V_S anomaly, δV_s (%).

most easily measured by comparing synthetic seismograms (PREM) against data (6). To avoid source location uncertainties, we compare P_d and S_d from the same event (Fig. 3*c*). The geometry is presented by Ni and Helmberger (18), where the phases cross the boundary nearly at right angles to the structure. The observations display considerable scatter because the array is broad and the ray paths apparently encounter 3D variation, i.e., samples from the right side are ≈1.5 s smaller than those from the left. In short, the dynamic model captures some of this level of observed variation indicative of a convecting region.

There are many advantages in sampling an unknown structure with paths following the same great circle as described earlier (Fig. 1*a*). Here, we display S_CS-S and P_CP-P for a Sandwich

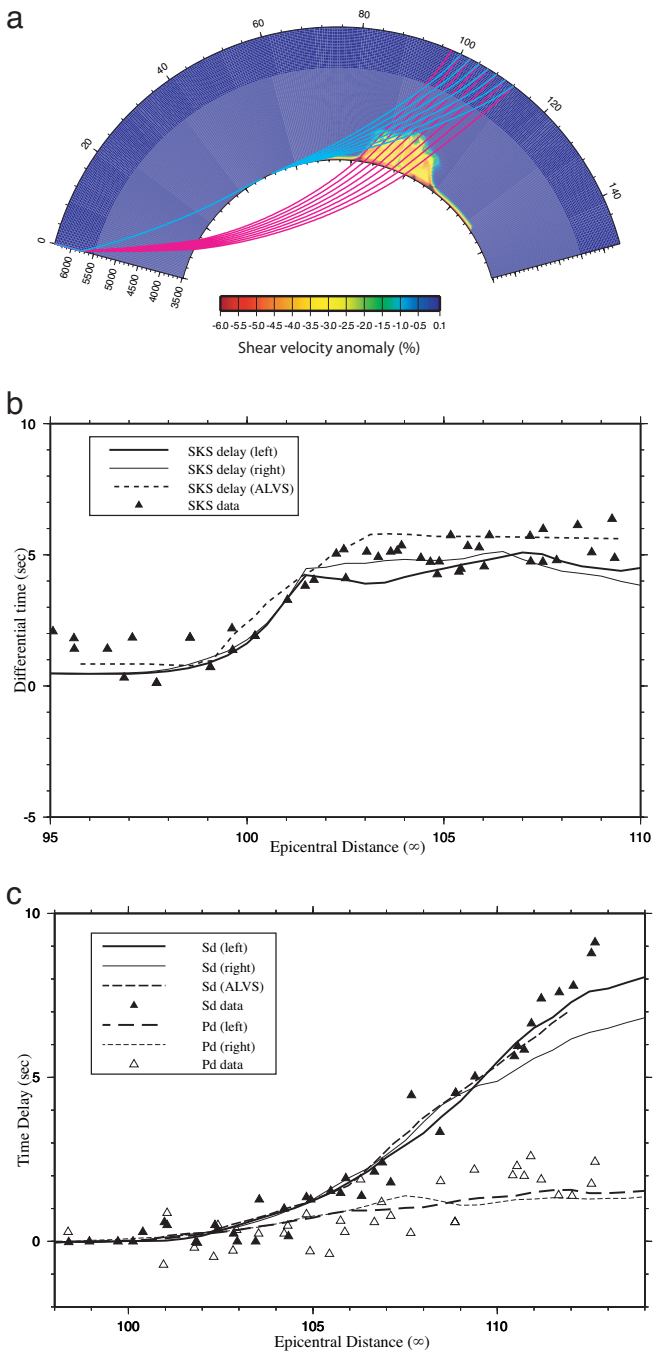

Fig. 3. Presentation of seismic predictions by inserting the HBMS model into the earth beneath Africa, essentially replacing Fig. 1*b* by Fig. 2*d* and comparing results against seismic observations. We have included the ALVS results for comparison. (*a*) The geometry and ray paths along a 2D cross-section (East Pacific Rise to the South Africa Array) sampling the anomalous structure, SKS (red) and S_d (light blue). (*b*) The differential timing derived by cross-correlating the observed waveforms (5), with synthetics relative to predictions from the 1D reference earth PREM. Because the structure is roughly symmetric, we included predictions from both sides with those from the left (heavy line) and from the right (light line). (*c*) A comparison of travel time predictions generated from HBMS synthetics against those observed at the South Africa Array (Kaapvaal array) (11) are displayed for diffracted S (S_d, ▲) and P (P_d, △). Because the diffracted waves sample the top edge of the structure first, the anomalous travel times have a gradual onset as predicted by the solid curves, heavy from the left, light from the right. Both the data and synthetic predictions display considerable scatter indicative of possible embedded fine structure, which is likely to be time-dependent. However, the magnitude of the anomalous S delays relative to P are well matched.

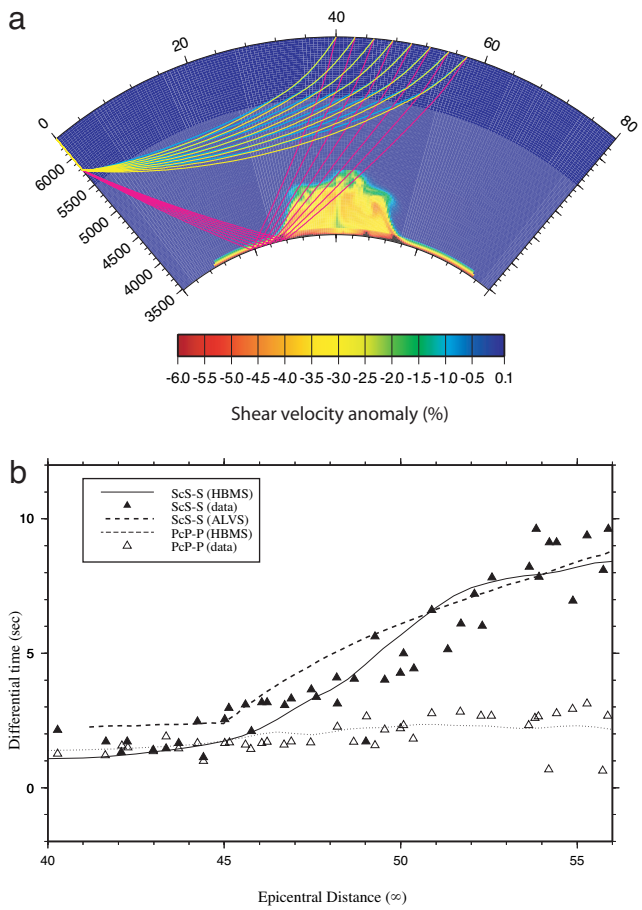

Fig. 4. Comparison of S_CS-S and P_CP-P predictions with observations (5). (*a*) The ray paths of S_CS (mangenta), S (cyan), and P (yellow) are shown sampling the HBMS model. (*b*) Comparison of differential S_CS-S (solid line) and P_CP-P (dot line) predicted by the HBMS and ALVS models. The modeled P_CP-P differential time is shifted up by 1 s, considering the possible base-line shift for origin time correction.

Island event (Fig. 4). The P and S direct rays encounter gentle mantle structures as explored with various tomographic maps (6). Thus, the differential times remove the timing errors associated with origin time and location and provide an accurate differential measure between the P and S velocities inside the anomalous structures. Note that the SKS delays fix the position of the wall, simplifying the interpretation of the S_CS-S delays and their increase with distance. The data scatter relative to the model similar to the S_d, suggesting complexity in the upper boundary.

Possible Phase Boundary

While Sandwich Island events produce excellent P_CP and S_CS recording on the South African Array, they also produce samples of the CMB directly below South Africa (Fig. 5) as recorded by the recently released Ethiopia/Kenya array data (19). Because this data set is rather unique, we will display the record section and predictions from both the ALVS and HBMS models and suggested model changes involving a possible PV-to-PPV phase change. The geometry is shown in Fig. 5*a* where SKS piercing points are denoted at the edges of the Superplume. The boundaries as discussed earlier are given as heavy dashed green lines. The S_CS bounce points are near the center of the structure where the down-welling developed in Fig. 2*d*. Record sections display the waveforms containing the various seismic arrivals with SKS

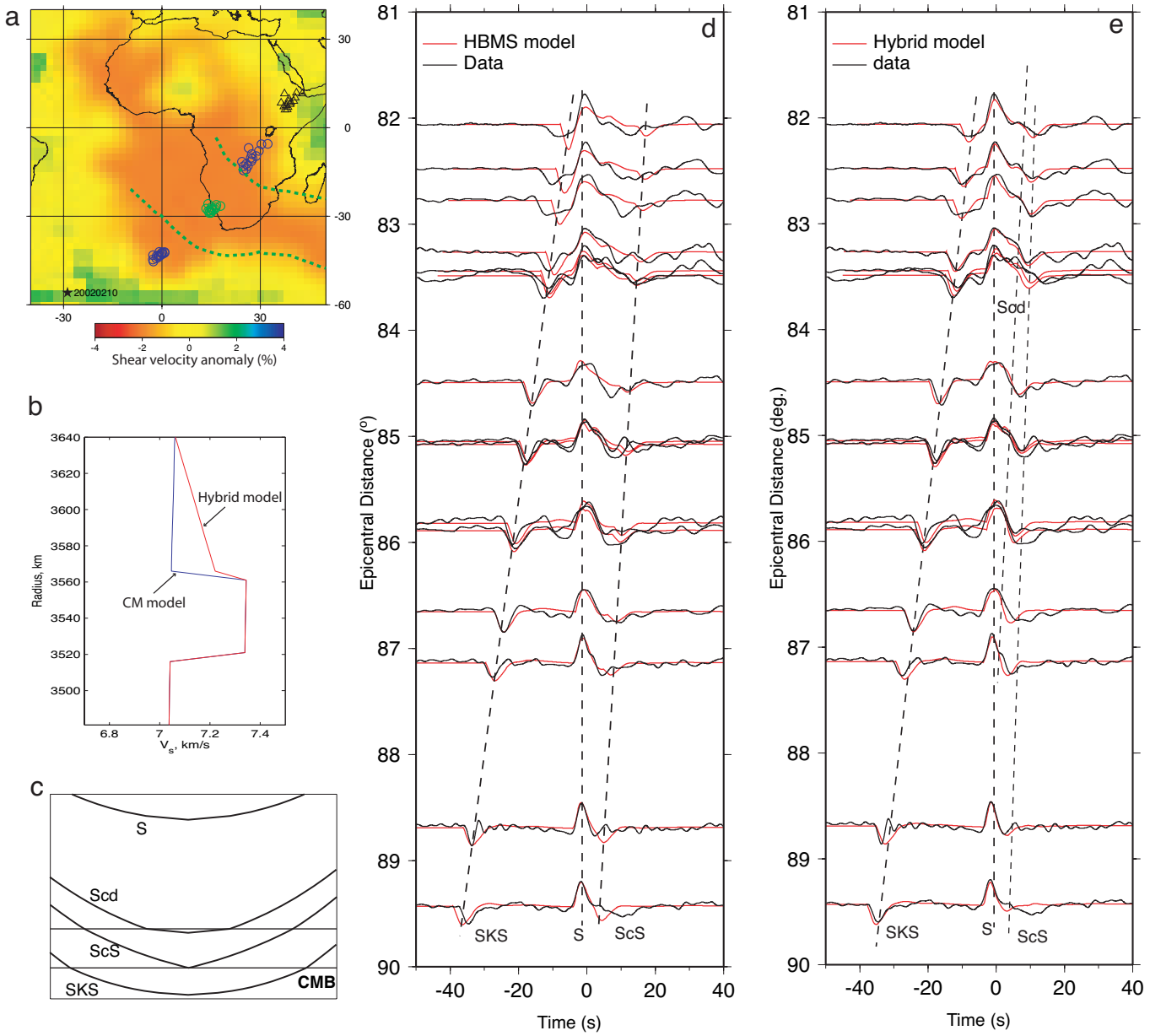

Fig. 5. Modeling a D″ triplication from the Ethiopia/Kenya array from a deep Sandwich Island event. (*a*) The recording geometry with solid circles indicating the S_CS sampling points at the CMB. (*b*) We assume that the ALVS inside the green box in Fig. 1*b* is 1D and replace the velocities near the bottom with our preferred structure (*b*). We have included a model with a sharp 4% jump (CM), which is discussed in *SI Text*. (*c*) Geometric ray paths with arrival times given as lines on the data-synthetic record sections. (*d*) The comparison with observed waveforms against predictions from the HBMS model. (*e*) The comparison with observed waveforms against predictions from the hybrid model containing structure *b*.

arriving first followed by S and ending with S_CS. The cross-over from S to SKS occurs ≈2° early relative to PREM because of the delayed S, which is common for the African anomaly (18).

Record sections relative to predicted PREM times are similar to these except there are some small station timing offsets. These small misalignments can be avoided by aligning directly on the peak of the S pulse as displayed in the record sections Fig. 5 *d* and *e*. Synthetic prediction for HBMS reproduces observed arrivals reasonably well, except that the differential time between S and SKS is small at smaller ranges and S_CS is late and complicated. In addition, there is a small arrival between S and S_CS having the timing expected for the Scd phase. This extra arrival is produced by a small triplication near the CMB, which appears between S and S_CS at ranges 80° to 90° (1). Because HBMS does not have such a phase boundary, we experimented with the original ALVS structure (Fig. 1*b*). We added a linear gradient to mimic the down-welling followed by a small velocity jump (1.7%), a strategy used earlier by Sidorin *et al.* (20). We conducted a grid search to derive the hybrid model (Fig. 5*b*) and synthetics displayed in Fig. 5*e*. The small pulse with a phase velocity slightly higher than S-labeled Scd is associated with this sharp boundary. The overall fattening at ranges 83° to 87° is caused by the high velocity gradient that is also present in the HBMS model. A slight adjustment in the timing of S has also been included as discussed in SI Figs. 8–10 to solve the small shift in cross-over present in Fig. 5*d*. Unfortunately, it proves difficult to sample D″ beneath the superplumes because of the strong constrains of station geometry. Thus, we do not know whether

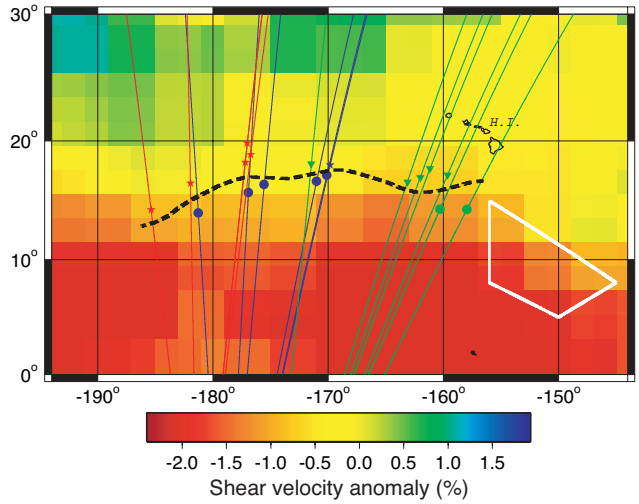

Fig. 6. Map of the northern edge of the Pacific Superplume displaying where anomalous seismic data has been studied relative to Grand's tomographic model (27). The rectangle indicates the position of a sharp change in shear velocity structure, which appears to be quite compatible with the edge of the HBMS (22). The piercing points of PKP(AB) three Fiji-Tonga events (red, green, and blue) are indicated relative to a dotted line where the dotted PKP arrivals are 2 s earlier than those to the north. The symbols indicted by * or triangles are locations where PKP(AB) display complexities (multipathed). The white trapezoid region shows rapid lateral variation of D″ (23).

the structure presented is related to the down-welling or even if it is PV to PPV, perhaps PPV to PV. Note that Tsuchiya and Tsuchiya (21) suggest that the PV-to-PPV transition for Fe-rich chemistry is likely to be accompanied by a negative V_S jump, which implies that a positive V_S jump then becomes a PPV-to-PV transition. However, considerable support for a positive velocity jump comes from studies near the Pacific superplume edge (22, 23), along with very strong lateral variations in S-velocity structure (Fig. 6). Strong variation in P-velocities has also been found near this same edge (24).

Edge Effects on P-Waves

Although the V_P anomalies are small for the LLVPs on average, the possible existence of sharp V_P features occurring near their edges is poorly imaged seismically because of the lack of differential phases. P_CP-P is not available for distances beyond 70° where the reflection coefficient (P_CP) becomes very small. Differential times, δt_k, between PKP(AB) and PKP(DF) has proven useful in studying D″ with some success (25). Because the AB and DF paths only separate in the lower mantle (see SI Fig. 11), their δt_k becomes a useful measure of lateral variation. Some sharp jumps in δt_k have been observed with no obvious explanation (Fig. 6). Fig. 6 displays the CMB piercing points for the phase PKP(AB) for events beneath the Tonga-Fiji Islands as recorded in Spain (24). The dotted line in Fig. 6 separates normal arrival times from late arrivals (2 s). It appears that these jumps in δt_k can be explained by the anomalous edge structure along the HBMS. Moreover, many observations north of the dotted line in Fig. 6 display waveform complexities that can be modeled by including ultralow velocity zones (ULVZs) (24). The most probable cause of the ULVZ is partial melting at the base of the mantle (26). Although the HBMS model did not include the melting process, the edges of the HBMS are substantially hotter than elsewhere, which become candidate locations for such zones.

Summary

In conclusion, we have tested a dynamic model HBMS by mapping excess T and density into V_P and V_S and comparing data against predicted synthetics. Not only did the dynamic model predict accurate results generated from the model, it suggests additional features that appear to be observable, such as plumes along the edges and a fast lens near the CMB, D″. An observed record section sampling beneath the Superplume can be modeled by assuming a velocity gradient (fast lens) and a 1.7% jump in S velocity situated 90 km above the CMB. However, because the above mapping strongly depends on assumed perturbations of the shear modulus to changes in T and composition, we have a self-compatible model that lacks uniqueness. The next step is to add the mineral physics constrains and retest all of the appropriate data sets. We would then be in position to better understand the dynamics behind some of the largest coherent structures in the mantle.

We thank two anonymous reviewers for helpful discussion and comments, which improved this article. The waveform data were obtained from Incorporated Research Institutions for Seismology. This work was supported by National Science Foundation Grant EAR-0456433.

1. Helmberger DV, Lay T, Ni S, Gurnis M (2005) *Proc Natl Acad Sci USA* 102:17257–17263.
2. Su WJ, Dziewonski AM (1997) *Phys Earth Planet Inter* 100:135–156.
3. Masters G, Laske G, Bolton H, Dziewonski AM (2000) in *Earth's Deep Interior: Mineral Physics and Tomography From the Atomic to the Global Scale*, eds Karato S, Forte AM, Liebermann RC, Masters G, Stixrude L (Am Geophys Union, Washington, DC), Am Geophys Union Geophys Monogr 117, pp 63–87.
4. Wang Y, Wen LX (2006) *J Geophys Res*, 10.1029/2006JB004483.
5. Helmberger DV, Ni SD (2005) in *Earth's Deep Mantle: Structure, Composition, and Evolution*, eds van der Hilst RD, Bass JD, Matas J, Trampert J (Am Geophys Union, Washington, DC), Am Geophys Union Geophys Monogr 160, pp 63–81.
6. Ni SD, Helmberger DV (2003) *Earth Planet Sci Lett* 206:119–131.
7. Ni SD, Tan E, Gurnis M, Helmberger DV (2002) *Science* 296:1850–1852.
8. Christensen U (1984) *Ann Geophys* 2:311–319.
9. McNamara AK, Zhong S (2004) *J Geophys Res*, 10.1029/2003JB002847.
10. Tan E, Gurnis M (2005) *Geophys Res Lett*, 10.1029/2005GL024190.
11. James DE, Fouch MJ, VanDecar JC, van der Lee S (2001) *Geophys Res Lett* 28:2485–2488.
12. Wen L (2001) *Earth Planet Sci Lett* 194:83–95.
13. Ni SD, Helmberger DV (2003) *J Geophys Res*, 10.1029/2001JB001545.
14. Tan E, Gurnis M (2006) *J Geophys Res*, 10.1029/2006JB004505.
15. Ni SD, Ding XM, Helmberger DV (2000) *Geophys J Int* 140:71–82.
16. Ristema J, Ni SD, Helmberger DV, Crotwell HP (1998) *Geophys Res Lett* 25:4245–4248.
17. Wen L, Silver P, James D, Kuehnel R (2001) *Earth Planet Sci Lett* 189:144–153.
18. Ni SD, Helmberger DV (2003) *Phys Earth Planet Inter* 140:243–251.
19. Nyblade AA, Langston CA (2002) *EOS Trans AGU* 83:405–408.
20. Sidorin I, Gurnis M, Helmberger DV, Ding XM (2001) *Earth Planet Sci Lett* 163:31–41.
21. Tsuchiya T, Tsuchiya J (2006) *Geophys Res Lett*, 10.1029/2006GL025706.
22. Lay T, Hernlund J, Garnero EJ, Thorne MS (2006) *Science* 314:1272–1276.
23. He YM, Wen LX, Zheng TY (2006) *Earth Planet Sci Lett* 244:302–314.
24. Luo SN, Ni SD, Helmberger DV (2001) *Earth Planet Sci Lett* 189:155–164.
25. Song XD, Helmberger DV (1993) *Geophys Res Lett* 20:285–288.
26. Garnero EJ, Revenaugh JS, Williams Q, Lay T, Kellogg LH (1998) in *The Core-Mantle Boundary Region*, eds Gurnis M, Wysession ME, Knittle E, Buffett B (Am Geophys Union, Washington, DC), Geodynamic Series 28, pp 319–334.
27. Grand SP (2002) *Philos Trans R Soc London A* 360:2475–2491.